LASER REMOTE SENSING OF COASTAL AND TERRESTRIAL POLLUTION BY FLS-LIDAR

Sergey Babichenko[1], Alex Dudelzak[2] and Larisa Poryvkina[1]

1. Laser Diagnostic Instruments Ltd., Tallinn; Estonia; ldi(at)ldi.ee
2. Laser Diagnostic Instruments International Inc., Ottawa, Canada; info(at)ldi3.com

ABSTRACT

The paper presents recent results of field experiments with airborne fluorescent lidar FLS-A based on excimer laser and multichannel detector. Helicopter installation was used to monitor water and land areas of oil transportation and storage. Techniques for real-time data acquisition and processing are described based on compiled and systematized library of LIF spectra of various underlying surfaces. The field tests have proved the ability of FLS-A lidar to distinguish the fluorescence of minor oil pollution on different spectral backgrounds usually recorded in airborne measurements. Further lidar developments are discussed.

Keywords: oil pollution, lidar, laser-induced fluorescence, remote sensing

METHODS

The FLS-lidar series is the family of laser remote sensing systems developed by Laser Diagnostic Instruments (LDI). These lidars were primarily developed for monitoring marine environments. Natural aquatic and terrestrial targets containing organic pollution and vegetation have been studied in numerous field experiments. The specificity of lidar applications in coastal shallow waters has been investigated with FLS-lidars operating at tuneable and fixed sensing wavelengths. Additional requirements on analytical lidar technologies have been determined due to specific measurement conditions: small depths of sensed water column; typically lower water transparency and higher amounts of suspended solids; effects of bottom and shore underlying surfaces on lidar echo signals. Further developments and field trials have shown that extending their application to diagnostics of chemicals on different types of underlying surfaces (water, soil, industrial sites, land and agricultural vegetation, etc.) is highly feasible.

The entire set of an FLS lidar includes a basic laser source with an integrated module of sensing wavelength converters, beam-transmitting and receiving telescopes, a highly sensitive, gated hyper-spectral optical receiver based on a flat-field polychromator, control electronics / processors, and operator's console. The FLS modular design enables easy replacement of the system's compatible units and change of the overall lidar configuration depending on the application. During several years of operating in the field, FLS lidars have been used on trucks, ships, airplanes, and helicopters to study and / or monitor various aquatic and terrestrial targets.

The FLS-A (airborne) lidar is based on excimer laser with non-stable resonator. A UV beam expander is used to decrease the beam divergence and to fulfil eye safety requirements. A gated intensified linear CCD - camera coupled with polychromator provides simultaneous read-out of Laser Induced Fluorescence (LIF) spectra and background subtraction (ambient and dark signals) as well as an optional signal accumulation feature to increase the signal-to-noise ratio. Due to the hyper-spectral detection system used in FLS, high-resolution LIF spectra can be obtained per laser pulse during both day and night operations. It allows a detailed analysis of spectral shapes of lidar echo signal to be performed. Switching of diffraction grating position enables spectral recording in two spectral ranges. Technical specs of FLS-A are shown in Table 1.

Due to its moderate weight and dimensions the lidar can be operated on board of small airplanes or helicopters at the sensing distances ranging from 50 to 300 m. FLS-A lidar operation is fully automated due to integrated control and data processing software, which operates in unattended

and operator mode. It includes mission planning, visualization of the flight trajectory and aircraft position on the digital map, real-time data acquisition and analysis, post-processing, and reporting. Every measured LIF spectrum is accompanied with GPS data and operational parameters of the lidar. The present paper overviews the application of FLS-A lidar on board of airplanes and helicopters for monitoring aquatic and terrestrial targets.

Figure 1: FLS-A lidar installation on board of MI-8 helicopter

Table 1: FLS-A lidar specification

Lidar parameters	Sensing wavelength	308 nm
	Pulse energy	120 mJ
	Repetition rate	25 Hz
	Detection spectral ranges	300-600/450-740 nm
	Number of detector channels	500
Operational data	Mains voltage	110/220 V, 60/50 Hz; 28V DC
	Power consumption	1100 VA
	Dimensions B x H x T	700 mm x 1396 mm x1016 mm
	Weight	180 kg

RESULTS

Remote diagnostics of oil pollution in seawater

Detection and quantification of oil pollution in water are two of the developed airborne lidar applications. Environmental protection requires monitoring of water areas where sudden pollution or its continuous accumulation may result in water quality degradation. Accumulation of minor releases of oil pollutants, fertilizers, etc. in water leads to disintegration of aquatic bioms, eutrophication, and the overall environmental decay. The lidars used for this purpose have mainly been aimed at detecting oil spills on the water surface and operated with discrete channel detector systems consisting of a set of photomultiplier tubes (1,2). FLS-lidars have proved to be very efficient in detecting and quantifying oil films of low thickness with the accuracy better than 0.05 μm (3), although their main advantage is the ability to detect trace pollution in water at concentration levels of *ppm* and lower.

Diagnostics of oil pollution in open sea and coastal waters differs by measurement conditions. For the open sea areas the Raman scattering (RS) signal is mainly affected by water turbidity and

roughness of water surface, which typically do not have small-scale spatial variability. Therefore, the fluorescent factor calculated as a ratio of fluorescence intensity to RS can effectively serve as a measure of Dissolved Organic Matter (DOM) and contamination quantity (4). Oil films on the water surface change the shape of LIF spectra as compared to uncontaminated water spectra by simultaneous increase of fluorescence intensity and decrease of the Raman-line intensity. Oil emulsion in water reveals itself as an additional structure in LIF spectra overlapping with the wide fluorescence band of DOM (5).

In coastal waters measuring conditions for laser remote sensing are different compared with open waters due to smaller depths of the sensed water column, typically lower water transparency, and larger amounts of suspended solids. The spatial variability of optical parameters in coastal waters is typically higher than in the open waters due to shore drainage and river discharges in addition to local hydrodynamic processes. In shallow waters the lidar echo signal can also be influenced by bottom and shore underlying substances. Sea surf can wash ashore and accumulate chemical pollution. In such spots the RS is often not visible at all. For this specific case the method of DOM spectra asymmetry calculation has been proposed to measure spatial trends of chemical pollution in shallow waters (5). Interpretation of LIF spectra under such variable conditions requires a comprehensive analysis of minor changes in spectral shapes of characteristic bands of lidar echo signal, which can be done in a most effective way using hyper-spectral detection.

Figure 2 shows an example of RS profile along the helicopter flight trajectory within the Tallinn coastal area. The Tallinn Bay, where the passenger port is located, surrounds the west coast of Viimsi peninsula and the cargo harbour and oil transit terminals with pipelines to load the tankers are located to the east of the peninsula.

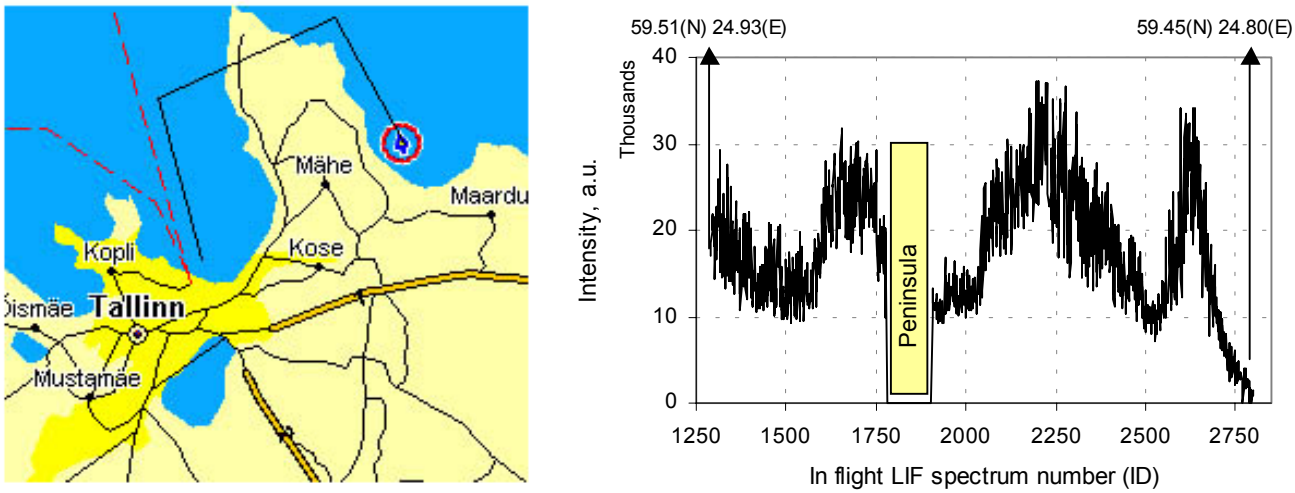

Figure 2: Left: Area map with helicopter flight route (solid line) and start position (red circle), passenger and cargo/oil harbours are marked, dashed lines show the regular routes of the ships. Right: Integral intensity of Raman scattering signal profile along the flight route.

The flight was performed at an altitude of 150 m with an average speed of 130 km/h. The LIF spectra were registered at every laser pulse, and the spatial resolution on the ground was about 5 m. The Raman signal varied significantly in the area with expressed spatial patches. Indeed, a decrease of RS was observed due to shallow waters along the east coast of the peninsula (see Figure 2, in flight LIF spectrum numbers ID: 1400-1600). When entering the open sea area, the values of RS increased twice (ID: 1600-1700). Shallow waters at the west coast also influenced the lower RS signal (ID: 1900-2100). In the central part of Tallinn Bay (ID: 2100-2300) the RS signal increased up to the level typical of open sea areas. A clear depression of RS intensity was observed when the flight trajectory crossed the routes of regular ferries (ID: 2300-2600). Due to intensive navigation the water was characterized by much higher turbidity than in other sections of the flight track. When moving towards the coast, RS jumped to its average level and started to decrease down to zero (at depths lower than 1 m).

This interpretation of RS signal variability is confirmed by an analysis of LIF spectra recorded in flight. For a more reliable analysis the real-time spectra are numerically filtered prior to processing. Figure 3 shows the difference in shape between filtered data (2-4) and raw data (4). Optimal filtration allows the noise level to be decreased while keeping all major spectral bands in place and in proper shape. Spectrum 1 in Figure 3 is typical of clean water in the open sea area. It is characterised by the highest level of RS and symmetric spectral shape of DOM fluorescence. Spectrum 2 was taken from the range corresponding to higher turbidity waters (crossing the ship routes). It is characterized by a proportional decrease of RS intensity and DOM fluorescence intensity due to lower transparency of water. Important is that the LIF spectral shape is exactly the same as for open sea. It confirms that there is no pollution in spite of the fact that the RS intensity decreases. The same interpretation can be given for shallow waters (spectrum 4), although the fluorescent factor is higher compared to the open sea, indicating a higher content of natural organic materials in the water.

By way of contrast, recorded LIF spectral shapes in the oil terminal area were different compared to previous examples (spectrum 3 in Figure 3). Indeed, an additional shoulder in UV range was revealed, typical of oil emulsions in water. Additionally, the spectral shape of the DOM fluorescence band was broadened out with a minor blue shift of the wavelength of maximal intensity. Such changes in shape of the LIF spectrum indicate the presence of low-level (below 1 *ppm*) pollution in water (v). Figure 4 shows the spatial trend of water contamination represented by the values of DOM spectra asymmetry.

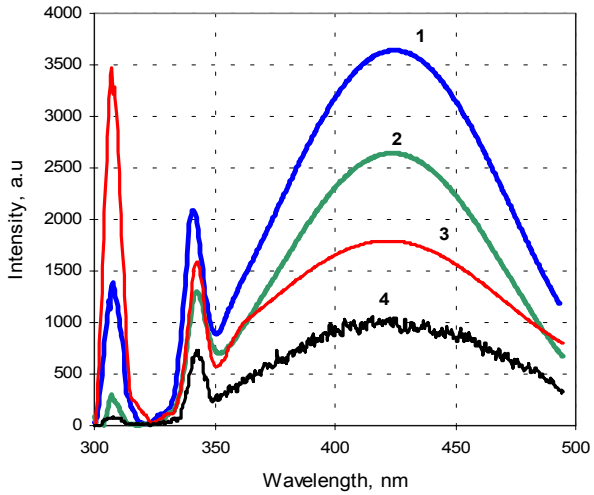

Figure 3: The examples of LIF spectra collected in flight: processed spectra of open seawater (1), coastal water (2), polluted water (3), and shallow water (4 – raw data).

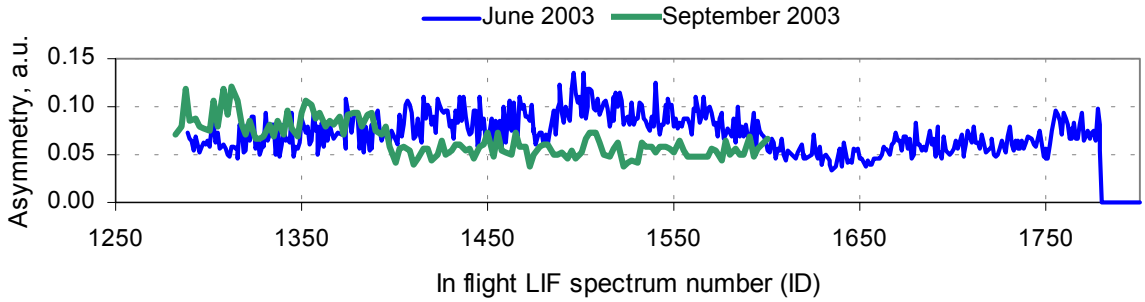

Figure 4: Asymmetry values near the harbour area in 2002 and 2003.

It should be mentioned that increased values of asymmetry due to trace pollution were repeatedly observed in the area of the cargo/oil harbour (compare data of 2002 and 2003, Figure 4). When on-line data processing takes place, it is a task for the lidar expert system to recognize and inter-

pret the changes in shape of LIF spectra. In marine applications the shapes of major spectral bands in LIF spectrum are well known. The task is more complicated when terrestrial targets are sensed.

Laser remote sensing of terrestrial targets

Applying the LIF method in airborne surveillance of terrestrial targets requires the spectral responses of different underlying surfaces to be understood. The corresponding reference library of LIF spectra has been compiled through continuous operations of a FLS-A lidar. The spectra were recorded in flights with simultaneous parallel visual classification of underlying surfaces. Examples of LIF spectra from the library in the spectral range of 310 – 610 nm are shown in Figure 5.

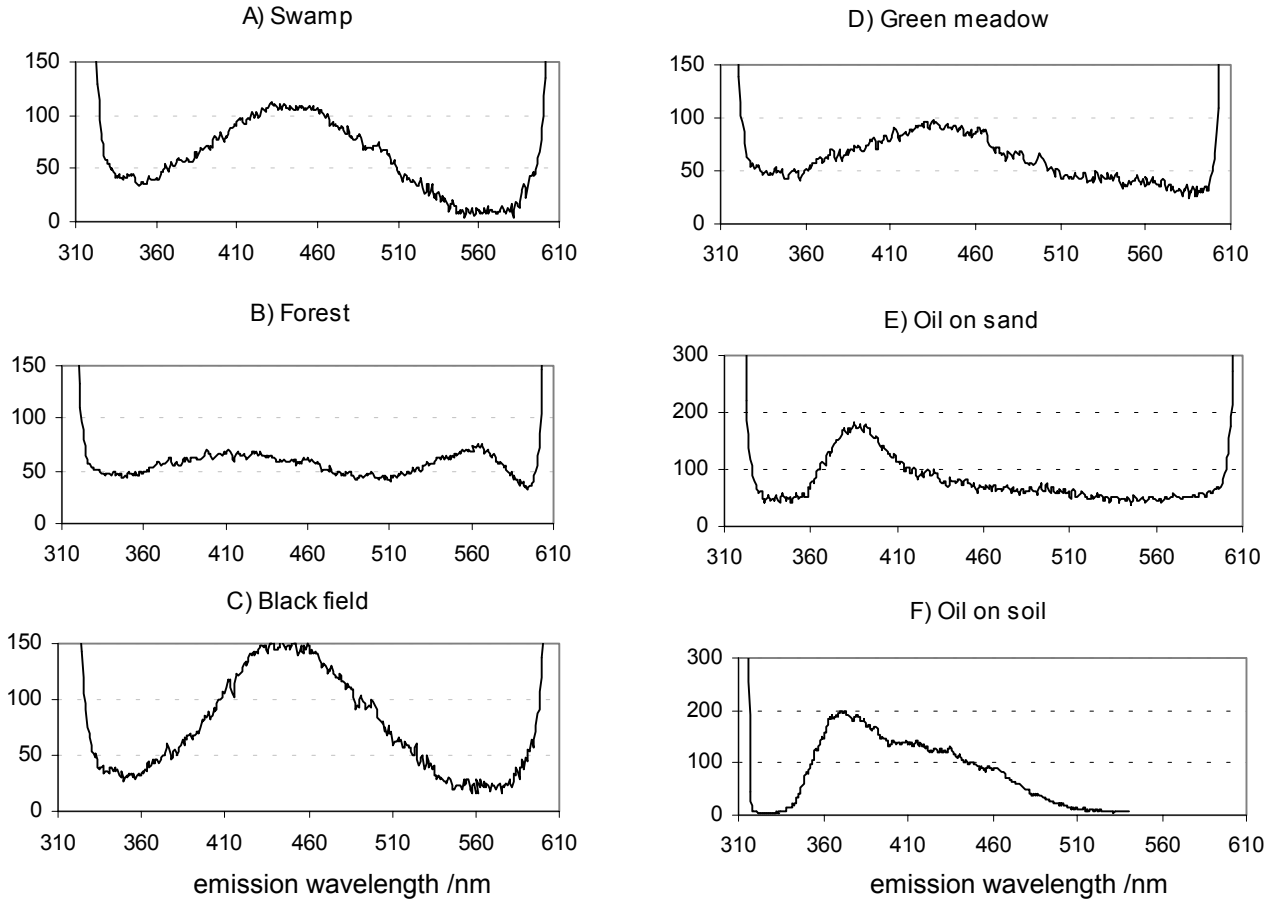

Figure 5: Examples of LIF spectra of underlying surfaces collected in flight.

Intensive lines at the left and right edges of the spectra correspond to the first and second spectral order of laser emission scattered by the underlying surface (unfiltered laser line). LIF spectra of sea natural water were described earlier. Swamp surface responds with fluorescent signals of humus (Figure 5a) with the typical red shift of the maximum in the fluorescence spectrum. The predominant high-molecular weight fractions in the composition of humic substances are responsible for this shift (compare with Figure 3, curves 1&2).

A similar spectrum is produced by an un-sowed agricultural field (Figure 5c). LIF spectra of green meadows and forests (Fig 5b,d) contain blue-green fluorescence bands reflecting a structure specific to higher plants (6). Red fluorescence of chlorophyll was detected in the 450 – 750 nm spectral range. Oil pollution patches on sand (e.g. seawater pollution washed ashore) are manifested as a spectral structure in fluorescent response between 360 and 480 nm (Figure 5e). The fluorescence of oil emulsion on soil overlaps with humus fluorescence (Figure 5f).

The field trials with FLS lidars have demonstrated their capability of sensing chemical pollutions on different types of underlying surfaces. The tests were carried out with airborne FLS-A lidar over

facilities such as oil storage tanks, railway oil transportation tanks and soils possibly contaminated with oil or oil products.

Figure 6 shows spectra consequently recorded from a helicopter flying over a railway train of oil tanks (flight speed 150 km/hour; altitude 150 m) per laser pulse. Traces of fresh oil patches were responsible for the short-wavelength part of fluorescence spectra, while the long wavelength edge corresponded to the old, degraded leak run-offs or patches.

No concentration estimations were made in flight. However, as tanks were freshly washed, most of the detected patches / run-offs were not visible to a naked eye. Thus, volume concentrations must have been very low. Nevertheless, all recorded fluorescence signals of oil leaks had higher intensities than corresponding values in the LIF spectra of underlying surfaces (see Figures 6,7). Spectrum A (Figure 6.) corresponded to minor pollution on the ground (invisible oil patches). Spectrum B reflected an old oil leak on the tank surface. Spectrum C indicated a fresh leak, and spectra D&E corresponded to a combination of fresh and old leaks. Similar spectra were recorded when flying over oil terminals, where oil patches could not be perceived by eye, either.

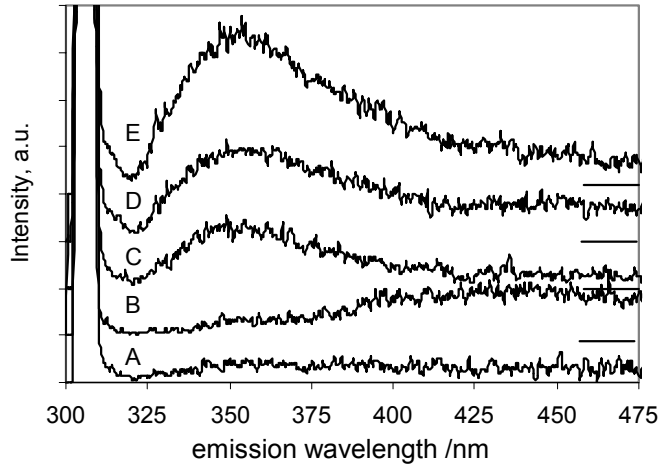

Figure 6. LIF spectra of railway oil tanks recorded with FLS-A lidar at 150 m flight altitude (see text for details).

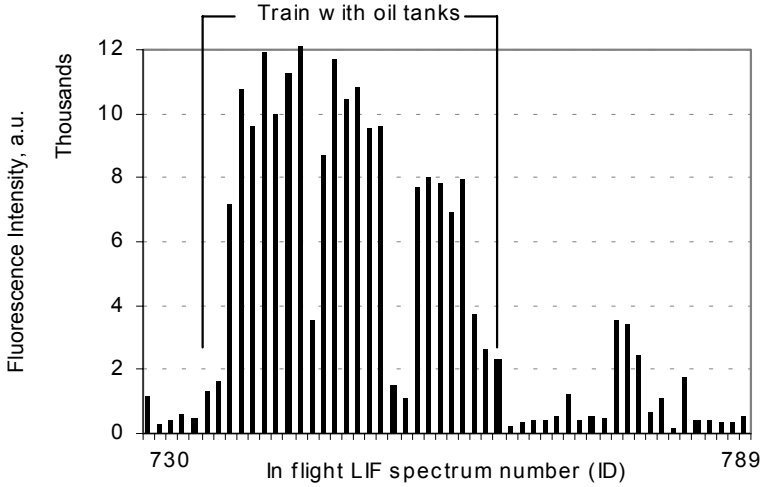

Figure 7. Fluorescence of minor oil run-offs on railway oil tanks. Integrated LIF spectra over the spectral range 320-400 nm.

Modelling experiments were performed to identify the concentration levels detectable under typical flight conditions described above. The experiments confirmed that the FLS-A is able to detect mi-

nor oil pollution on the ground (less than 1 ml of oil per m^2) from flight altitudes of up to 200 m and at an aircraft speed of 150 km/hour and demonstrated the potential of using FLS-A lidars as an oil pipeline monitoring tool.

CONCLUSIONS

The presented results of field experiments with the FLS-A lidar confirm that such a system is ready to be implemented in operational use for remote sensing of aquatic and terrestrial targets. The analytical capability of laser remote sensing system depends strongly on the optimisation of the hardware set-up and on a proper choice of the data processing technique. The expert system of FLS-lidars is able to classify LIF spectra and interpret minor changes in their shape. This is a step forward towards the recognition of lidars as analytical instruments rather than remote detection tools.

A strong demand can be expected soon for routinely operated, cost-effective remote sensing instrumentation with analytical capabilities that can be placed on small stationary, ground-moving, airborne, aquatic or terrestrial platform. The FLS modular design offers a solution adaptable to a variety of such platforms from small planes or helicopters to *in situ* and stand-off stationary systems. Current developments of FLS lidars aim at implementing a laser beam scanning system, which will allow a swath to be made on the ground by laser beam and the position of a local small-scale pollution to be precisely detected. This option is especially important for applications of laser remote sensing in pipelines environments.

ACKNOWLEDGEMENTS

The authors are grateful to the research and engineering staff of Laser Diagnostic Instruments and to the helicopter crew of the Estonian Air Force.

REFERENCES

1 Hengstermann T & R Reuter, 1990. Lidar fluorosensing of mineral oil spills on the sea surface. Applied Optics, 29: 3218 – 3227

2 Brown C E, R Nelson, M F Fingas & J V Mullin, 1997. Airborne laser fluorosensing: overflights during lift operations of a sunken oil bargade, In: IV Thematic Conference Remote Sensing for Marine and Coastal Environments, (Orlando, FL), 1: 23-30

3 Patsayeva S, V Yuzhakov, V Varlamov, R Barbini, R Fantoni, C Frassanito & A Palucci, 2000. Laser spectroscopy of mineral oils on water surface. EARSeL eProceedings, 1: 106-115

4 Klyshko D N & V V Fadeev, 1978. Remote Detection of Water Admixtures by Laser Spectroscopy with Raman Scattering Calibration. Doklady AN SSSR, 238: 320-323

5 Babichenko S, A Dudelzak & L Poryvkina, 2002. Laser sensing technologies in studies of marine and coastal environment. In: Seventh International Conference on Remote Sensing for Marine and Coastal Environments, (Miami, FL), eProceedings, Veridan, 8 p.

6 Babichenko S, A Dudelzak, G Samson, N Tremblay & J Wollring, 2000. Nutrient Stress of Corn Plants: Early Detection And Discrimination Using a Compact Multiwavelength Fluorescent Lidar. EARSeL eProceedings, 1: 224-233